Inorg. Chem. **2008**, *47*, 10723−10728

Submicrosized Rods, Cables, and Tubes of ZnE (E = S, Se, Te): Exterior−Interior Boron-Chalcogen Conversions and Optical Properties

Yi-Zhi Huang, Ling Chen, and Li-Ming Wu*

State Key Laboratory of Structural Chemistry, Fujian Institute of Research on the Structure of Matter, Chinese Academy of Sciences, Fuzhou, Fujian 350002, People's Republic of China

Received March 19, 2008

The submicrosized ZnE rods, ZnO/ZnE cables, and ZnE tubes (E = S, Se, Te) have been synthesized via exterior-to-interior boron-chalcogen corrosions on the initial ZnO rods. The products are well characterized by XRD, SEM, TEM, and elemental analyses. The morphologies of both ZnE rods and ZnO/ZnE cables are roughly comparable to that of ZnO. The measured optical gaps of the ZnE rods are in agreement with those of the corresponding bulk materials, and the ZnO/ZnE cables exhibit type-I excitonic localization that is restrained in the region of the narrower band gap component.

1. Introduction

Binary metal chalcogenides are attractive materials in many industrial applications owing to their fundamental optical, electronic, and magnetic properties. The syntheses of sulfides have been successful with the aids of the conventional sulfur sources, for example, H_2S, CS_2, A_2S (A = alkali metal), elemental S, and organic thio compounds.[1,2] However, the usual risks of such methods would be the release of harmful H_2S gas and the undesired incomplete sulfidation. The syntheses of selenides and tellurides, especially the nanosyntheses, are relatively rare, mostly because the selenium and tellurium sources have acute toxicity and are therefore difficult to handle. A few tellurium sources are utilized to generate nano chalcogenides via solution approaches, such as the tellurium element for Ag_2Te fibers,[3] Bi_2Te_3 particles,[4] and ZnTe rods,[5] and bis(*tert*-butyldimethylsilyl)tellurium [$(BDMS)_2Te$] or trioctylphosphine telluride [TOPTe] for CdTe quantum dots and so forth.[6] The extension of known methods to other metal tellurides is scarcely successful, partly because the low solubility of tellurium in aqueous solution, the undesired oxidation of tellurium, and the toxicity and cost of the organic tellurium reagents. Thus, safe, efficient, and inexpensive chalcogenidation reagents, especially telluridation reagents, are highly desired.

The newly established boron-sulfur-method is a convenient synthetic approach for a broad range of metal sulfides.[7] This unique technique utilizes the in situ boron sulfides as the sulfur source and thus exhibits several advantages in: 1) easier and safer handling because all of the starting reactants are stable at room temperature, that is, boron and sulfur elements and metal oxides or hydroxides; 2) minimum risk of harmful gas release because the reaction is carried out in a closed container; 3) applicability for a wide range of compounds including main group metal oxides, transition-metal oxides, and lanthanide oxides; 4) mild heating condition because the byproduct B_2O_3 is highly thermodynamically favored.

The previous reports have also demonstrated that the mild heating condition of such method benefits a neat shape retentive conversion, for example, nanodisk-to-nanodisk[8] or wire-to-wire[9] conversions of oxide/hydroxide to sulfide. Thus, the exploration of the similar B-Se and B-Te systems would be promising because the chemical similarity of selenium or tellurium with sulfur.

* To whom correspondence should be addressed. E-mail: Liming_wu@fjirsm.ac.cn.

(1) Muller, A.; Krebs, B. *Sulfur: Its Significance for Chemistry, for the Geo-, Bio-, and Cosmosphere and Technology*; Elsevier Science Publishers: Amsterdam, 1984.
(2) Stiefel, E. I.; Matsumoto, K. Transition Metal Sulfur Chemistry: Biological and Industrial Significance, *ACS Symposium Series, 653*; American Chemical Society: Washington, D.C., 1996.
(3) Mu, L.; Wan, J. X.; Ma, D. K.; Zhang, R.; Yu, W. C.; Qian, Y. T. *Chem. Lett.* **2005**, *34*, 52–53.
(4) Zheng, Y. Y.; Zhu, T. J.; Zhao, X. B.; Tu, J. P.; Cao, G. S. *Mater. Lett.* **2005**, *59*, 2886–2888.
(5) Li, Y. D.; Ding, Y.; Wang, Z. Y. *Adv. Mater.* **1999**, *11*, 847–850.
(6) Murray, C. B.; Norris, D. J.; Bawendi, M. G. *J. Am. Chem. Soc.* **1993**, *115*, 8706–8715.
(7) Wu, L. M.; Seo, D. K. *J. Am. Chem. Soc.* **2004**, *126*, 4676–4681.
(8) Wu, L. M.; Sharma, R.; Seo, D. K. *Inorg. Chem.* **2003**, *42*, 5798–5800.
(9) Huang, Y. Z.; Chen, L.; Wu, L. M. *Cryst. Growth Des.* **2008**, 739–743.

10.1021/ic8005053 CCC: $40.75 © 2008 American Chemical Society
Published on Web 10/15/2008

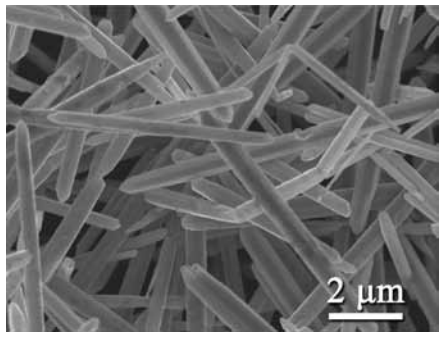

Figure 1. Typical SEM image of the submicrosized ZnO rods made by a modified solvothermal process.

In this article, we report the syntheses of the submicrosized ZnE rods, ZnO/ZnE cables, and ZnE tubes (E = S, Se, Te) via boron-chalcogen conversions on ZnO template. The optical band gaps of the products are measured by the diffuse reflectance spectra and the results of ZnO/ZnE cables nicely demonstrate the tunable excitonic localization in these heterostructures. Different from the linear ZnSe,[10−12] and wiry ZnTe,[5,13] the tubular morphology of ZnSe and ZnTe reported here together with the novel cables of ZnO/ZnSe, and ZnO/ZnTe have not been observed previously. Only the hollow ZnSe tubes has one related example that is randomly tin-filled made by a very different approach.[12]

2. Experimental Section

All of the chemicals were used as purchased without further purification. Amorphous boron (95%, Dandong Chemical Co.), sublimed sulfur (98%), selenium powder (98%), tellurium powder (99.9%), $Zn(Ac)_2 \cdot 2H_2O$ (99%), and Na_2CO_3 (99%) were all purchased from Sinopharm Chemical Co..

Synthesis of the Template, ZnO Submicrorods. The facile submicrorods of ZnO were chosen as the template to grow the desired zinc chalcogenides ZnE (E = S, Se, Te). The synthesis is fulfilled by a modified hydrothermal procedure[14] as briefly described as followed. A 96 mL of 0.08 M Na_2CO_3 solution of ethanol/water (1:1 v/v) was added drop wisely into 96 mL of 0.04 M $Zn(Ac)_2$ ethanol/water solution at 60 °C. The resulted suspension was transferred into a 240 mL autoclave with Teflon liner, heated at 150 °C for 10 h, and cooled radiantly to room temperature. The white precipitate was collected by centrifugation, washed with distilled water and ethanol, respectively, and finally dried in air. The as-prepared ZnO rods are mostly of 100−800 nm in width as shown in Figure 1 and used in all experiments described below without any size separation.

Syntheses of the ZnE Submicrorods (E = S, Se, Te). The suitable amount of ZnO rods was put in a silica tube (i.d., 1 cm, length, 2 cm) that was placed on the top of another identical silica tube loading with the stoichiometric boron and sulfur powder[7−9] (or B/Se, B/Te mixture). Such assembly was situated inside a slightly larger silica jacket, evacuated, and flame-sealed, and then gradually heated at a rate of 50 °C/h to the designated temperature, annealed for a certain time, and subsequently cooled radiantly to room temperature. The powdery product in the top tube was cleaned with CS_2 and ethanol for several times to get rid of the byproducts. The optimized synthetic conditions for ZnE submicrorods are profiled in Figure 2, and the corresponding results are listed in Table 1. The chemical reaction equation is established following our previous reports:[7−9]

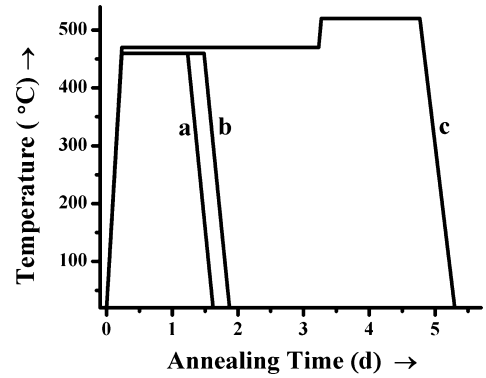

Figure 2. Optimized heating profiles for the complete chalcogenidation product submicrorods of (a) ZnS, (b) ZnSe, and (c) ZnTe.

$$\mathrm{ZnO} + \frac{2}{3}\mathrm{B} + \mathrm{E} \rightarrow \mathrm{ZnE} + \frac{1}{3}\mathrm{B_2O_3}(\mathrm{E} = \mathrm{S, Se, Te}). \quad \text{(I)}$$

Syntheses of the Submicrocables of ZnO/ZnE (E = S, Se, Te). The submicrocables with ZnO as core and ZnE as sheath were obtained via the incomplete chalcogenidation processes. The degree of the chalcogenidation is controlled via applying different experimental parameters, such as shorter reaction time, lower reaction temperature, or insufficient chalcogen reactants. The detailed experimental conditions for each ZnO/ZnE submicrocable are given in the text.

Syntheses of the Submicrotubes of ZnE (E = S, Se, Te). The above-made ZnO/ZnE submicrocables were immersed in a dilute HCl solution for several hours, and the expected ZnE tubes were thus produced because the solubility of ZnO is larger than that of ZnE. Such approach is similar to the report on ZnS tubes where sulfur element or H_2S are used as a sulfur source;[15] however, success on ZnSe or ZnTe tube has not been reported.

Sample Characterization. The phase identity and morphology of the products were characterized by powder X-ray diffraction (XRD; BDX3300), scanning electron microscopy (SEM; JSF-6700F), energy-dispersive X-ray spectrum (EDS), and transmission electron microscopy (TEM; JEM-2010). Elemental analysis was performed on a Vario EL III elemental analyzer for sulfur and on an Ultima-2 inductively coupled plasma optical emission spectrometer (ICP-OES) for selenium, tellurium, and zinc. The diffuse reflectance spectrum was recorded on a PerkinElmer Lambda-900 spectrophotometer.

3. Results and Discussion

3.1. Submicrosized ZnS Rods, ZnO/ZnS Cables, and ZnS Tubes. The submicrosized ZnS rods were made at 460 °C within 24 h. The XRD patterns shown in parts a and b of Figure 3 indicate that the initial wurtzite ZnO (JCPDS 36−1451) was completely converted into the wurtzite ZnS (JCPDS 36−1450). The elemental analyses on ZnS product

(10) Cozzoli, P. D.; Manna, L.; Curri, M. L.; Kudera, S.; Giannini, C.; Striccoli, M.; Agostiano, A. *Chem. Mater.* **2005**, *17*, 1296–1306.
(11) Jiang, Y.; Meng, X. M.; Yiu, W. C.; Liu, J.; Ding, J. X.; Lee, C. S.; Lee, S. T. *J. Phys. Chem. B* **2004**, *108*, 2784–2787.
(12) Hu, J. Q.; Bando, Y.; Zhan, J. H.; Liu, Z. W.; Golberg, D.; Ringer, S. P. *Adv. Mater.* **2005**, *17*, 975–979.
(13) Li, L.; Yang, Y. W.; Huang, X. H.; Li, G. H.; Zhang, L. D. *J. Phys. Chem. B* **2005**, *109*, 12394–12398.
(14) Huang, Q.; Gao, L. *J. Am. Ceram. Soc.* **2005**, *88*, 1403–1406.
(15) Dloczik, L.; Engelhardt, R.; Ernst, K.; Fiechter, S.; Sieber, I.; Konenkamp, R. *Appl. Phys. Lett.* **2001**, *78*, 3687–3689.

Table 1. Descriptions of ZnO Template and ZnE (E = S, Se, Te) Products[a]

sample (space group)	color of the sample	estimated lattice parameters	lattice parameters from JCPDS	JCPDS no.
ZnO ($P6_3mc$)	white	$a = b = 3.253(2)$ Å $c = 5.221(5)$ Å	$a = b = 3.250$ Å $c = 5.207$ Å	36−1451
ZnS ($P6_3mc$)	white	$a = b = 3.824(2)$ Å $c = 6.254(8)$ Å	$a = b = 3.821$ Å $c = 6.257$ Å	36−1450
ZnSe ($F43m$)	yellowgreen	$a = b = c = 5.668(0)$ Å	$a = b = c = 5.670$ Å	88−2345
ZnTe ($F43m$)	darkred	$a = b = c = 6.104(0)$ Å	$a = b = c = 6.103$ Å	15−0746

[a] X-ray powder diffraction pattern analysis and unit cell refinement were performed by the *JADE* program.

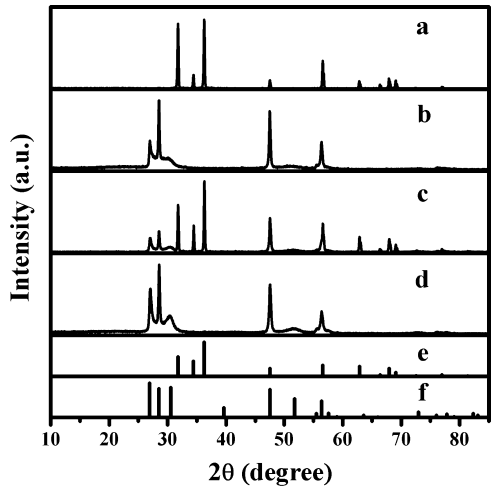

Figure 3. XRD patterns of (a) ZnO rods, (b) ZnS rods obtained at 460 °C for 24 h, (c) ZnO/ZnS cables obtained at 460 °C for 2 h, and (d) ZnS tubes after an acid etching. The standard patterns for (e) wurtzite ZnO (JCPDS 36−1451) and (f) wurtzite ZnS (JCPDS 36−1450).

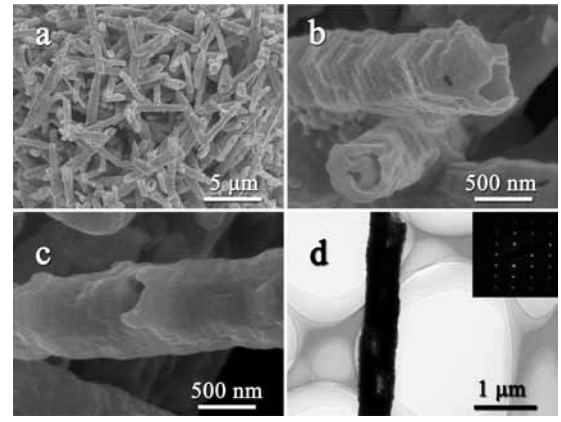

Figure 4. (a−c) Typical SEM images and (d) TEM image of the ZnS rods. The upper-right inset of the TEM image is the SAED pattern.

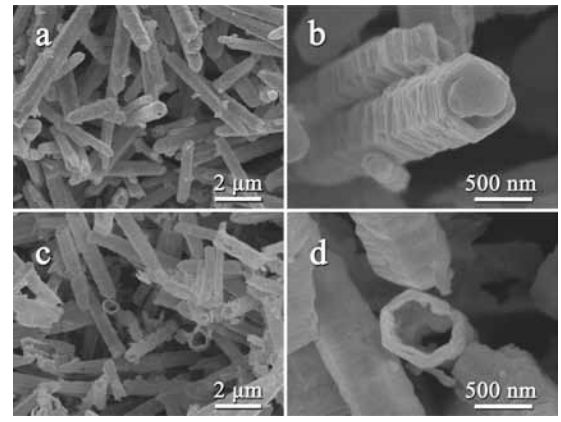

Figure 5. Typical SEM images of (a and b) ZnO/ZnS cables and (c and d) ZnS tubes.

give a molar ratio of Zn:S = 1.00:1.03, which suggests that the sulfidation is complete. The elemental analyses on ZnSe and ZnTe rods described below both indicate a molar ratio of Zn:E = 1.00:1.00, which also substantiate the complete conversions. Careful examination on the diffraction peaks reveals that the (002) diffraction peak of ZnS at $2\theta = 28.5°$ is sharper and stronger than the (100) and (101) peaks, which may suggest a preferred orientation along the *c* axis. Such orientation may be inherited from the initial ZnO, in which the sharpest (002) peak at $2\theta = 34.4°$ also indicates the orientation preference along *c* axis. This observation is similar as previous report.[16] The rod morphology of the ZnS is shown by a typical SEM image in part a of Figure 4. Although both the initial ZnO rods and the product ZnS rods feature 1D rodlike morphology, three marked differences are found before/after the B-S conversion: 1) a general increase in diameters for ZnS, which agrees with the expansion of the unit cells from ZnO to ZnS ($a = 3.250$ vs 3.821 Å, $c =$ 5.207 vs 6.257 Å); 2) perceptible surface roughness of the ZnS rods that may indicate a poor epitaxial crystallization under the influence of the lattice mismatch (16−18%); 3) porosity of ZnS rods, as shown by the high-magnification SEM (parts b and c of Figure 4). The holes might be caused by the migration of vacancies according to the Kirkendall effect in solid-state diffusion.[17] The porous rods are finely crystalline as indicated by a selected-area electron diffraction (SAED) pattern in part d of Figure 4.

Interestingly, shortening the reaction time is effective to interrupt the sulfidation process. The XRD pattern taken on the intermediate (part c of Figure 3) clearly displays the coexistence of ZnO and ZnS. Such coexistence has been proved by the element analysis result of Zn:S = 1:0.45. This indicates that about 45% of ZnO has been converted to ZnS. The intermediate also features a rodlike morphology, rough surface, hexagonal column outline, and size distribution (parts a and b of Figure 5) similar as those of the completely sulfidized ZnS product (Figure 4). The intermediate product was subsequently immersed in a dilute HCl solution for several hours, then washed and dried. The as-treated sample is pure ZnS phase (part d of Figure 3) and presents a hollow tubular morphology (part c of Figure 5). A few vertical tubes show a perspective view to the testing holder (part d of Figure

(16) Panda, S. K.; Dev, A.; Chaudhuri, S. *J. Phys. Chem. C* **2007**, *111*, 5039–5043.
(17) Paul, A. The Kirkendall Effect in Solid State Diffusion. Ph.D. Thesis, Eindhoven University of Technology: Eindhoven, 2004.

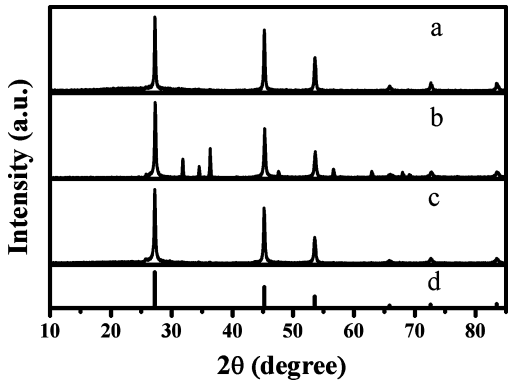

Figure 6. XRD patterns of (a) ZnSe rods obtained at 460 °C for 30 h, (b) ZnO/ZnSe cables at 460 °C for 12 h (with the loading ratio of ZnO:Se = 2:1), and (c) ZnSe tubes after acid etching. (d) The standard pattern for sphalerite ZnSe (JCPDS 88−2345).

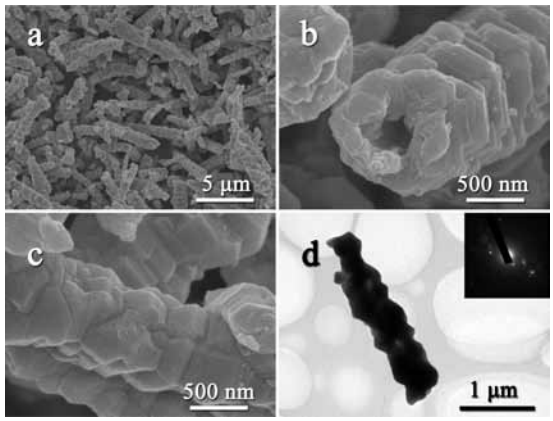

Figure 7. (a−c) Typical SEM and (d) TEM images of ZnSe rods. The upper-right inset of the TEM image corresponds to its SAED pattern.

5). Such ZnS tubes have size distribution and surface morphology comparable to that of the intermediate product. The absence of ZnO judging from the XRD (part d of Figure 3) and the disappearance of the core as shown in the SEM images (parts c and d of Figure 5) allow us to conclude that the intermediate product is heterostructure with ZnO as core and ZnS as sheath, that is, the ZnO/ZnS cable.

3.2. Submicrosized ZnSe Rods, ZnO/ZnSe Cables, and ZnSe Tubes. The selenidation of ZnO template has also been explored. In principle, the fully selenidation of ZnO requires moderately longer reaction time than the sulfidation does, 30 h at 460 °C versus 24 h at 460 °C. The XRD pattern of as-made ZnSe rods is shown in part a of Figure 6, which matches well with cubic ZnSe (sphalerite type, JCPDS 88−2345). The SEM and TEM observations (Figure 7) show that ZnSe also preserves the rodlike shape, and holds a larger diameter. Compared with ZnS rods, ZnSe rods have coarser surfaces (parts b and c of Figure 7 vs parts b and c of Figure 4) and poorer crystallinity (inset in part d of Figure 7 vs the inset in part d of Figure 4). Such phenomenon indicates a larger degree of the nonepitaxial crystallization during the selenidation process, which is a consequence of the lattice mismatch between sphalerite ZnSe and wurtzite ZnO.

An incomplete selenidation reaction was carried out by loading insufficient Se (ZnO:Se = 2:1 in molar) and anneal

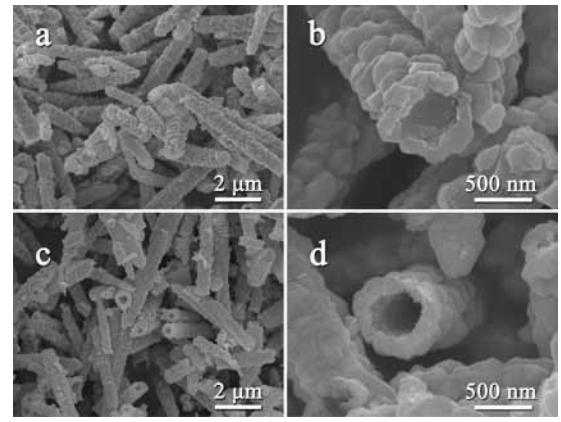

Figure 8. Typical SEM images of (a and b) ZnO/ZnSe cables and (b−d) ZnSe tubes.

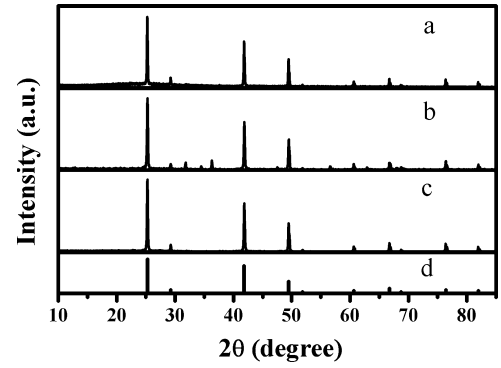

Figure 9. XRD patterns of (a) ZnTe rods obtained at 470 °C for 72 h and 520 °C for another 36 h, (b) ZnO/ZnTe cables obtained at 470 °C for 72 h, and (c) ZnTe tubes after an acid etching. (d) The standard pattern for sphalerite ZnTe (JCPDS 15−0746).

for a shorter time of 12 h at 460 °C. As expected, the corresponding XRD pattern on such intermediate product (part b of Figure 6) indicates the coexistence of ZnO and ZnSe; the SEM images (parts a and b of Figure 8) exhibit rodlike morphology. A subsequent acid etching of the intermediate resulted in the expected pure phase of ZnSe tubes (XRD in part c of Figure 6, SEM in parts c and d of Figure 8). Thus, the intermediate product is a ZnO/ZnSe cable.

3.3. Submicrosized ZnTe Rods, ZnO/ZnTe Cables, and ZnTe Tubes. The telluride extension has successfully produced the expected ZnTe rods and ZnO/ZnTe cables that further generate ZnTe tubes. The phase singularity of the ZnTe (JCPDS 15−0746) or the coexistence of ZnO and ZnTe is checked by the XRD patterns as shown in Figure 9, and the morphologies of the products are presented in Figure 10. The complete telluridation requires significantly higher reaction temperature and longer anneal time than the selenidation process does, that is, 36 h at 520 °C versus 30 h at 460 °C, and the telluridation process shows poorer morphology maintenance because the simultaneous formation of chunky product that partially responses for the destruction of the initial morphology. The chunks are made of only zinc and tellurium judging from EDS results. Compared with other chalcogen, tellurium has the highest melting point, 449 °C versus 221 °C of selenium and 96 °C of sulfur; thus, the initiation of the telluridation that is determined to some

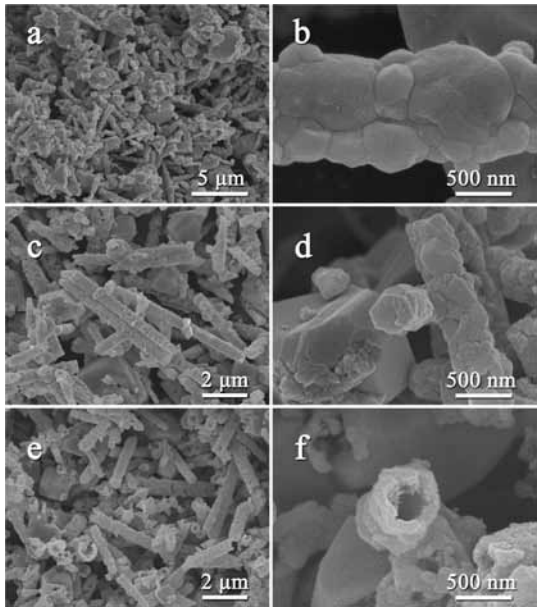

Figure 10. Typical SEM images of (a and b) ZnTe rods, (c and d) ZnO/ZnTe cables, and (e and f) ZnTe tubes.

degree by the formation of the gasous B_xTe_y species needs higher temperature. On the other hand, the bulk ZnTe has the lowest mp among the three zinc chalcogenides, 1718, 1526, and 1300 °C for hexagonal ZnS, cubic ZnSe, and ZnTe, respectively,[18] and the small ZnTe particles formed during the early reaction stage are likely to have lower melting point since the size effect,[19,20] thus the interparticle aggregations are accelerated to form the ZnTe chunks and thus partly destroy the 1D rod morphology of the initiate ZnO template.

3.4. Optical Properties of the Submicrosized ZnE Rods, ZnO/ZnE Cables, and ZnE Tubes (E = S, Se, Te). Zinc oxide and chalcogenides are wide band gap semiconductors with direct optical transitions. The direct band gap (E_g) can be determined according to the expression for the absorption coefficient (α) as a function of photon energy ($h\upsilon$):

$$\alpha = A(h\upsilon - E_g)^{1/2}/h\upsilon \quad (1)$$

where A is a constant.[21] The absorption coefficient is related to the reflectance (R) by the Kubelka−Munk function:

$$F(R) = (1-R)^2/2R = \alpha/S \quad (2)$$

If the dependence of the scattering coefficient (S) on the incident wavelength is neglected, the band gap can be estimated by extrapolating the linear portion of the absorption edge in a $(F(R)h\upsilon)^2$ against $h\upsilon$ curve to $(F(R)h\upsilon)^2 = 0$.[23,24] As illustrated in Figure 11, the band gaps of the rods of ZnO, ZnS, ZnSe, and ZnTe are estimated to be 3.25, 3.60, 2.65, and 2.24 eV, respectively. All are in good agreement with

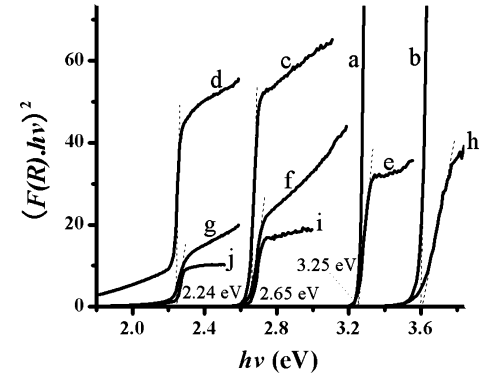

Figure 11. Diffusion reflectance spectra of (a) ZnO rods, (b) ZnS rods, (c) ZnSe rods, (d) ZnTe rods, (e) ZnO/ZnS cables, (f) ZnO/ZnSe cables, (g) ZnO/ZnTe cables, (h) ZnS tubes, (i) ZnSe tubes, and (j) ZnTe tubes.

the reported values for the corresponding bulk materials, and the descend trend ZnS > ZnO > ZnSe > ZnTe agrees with the previous reports.[25] The ZnE tube members show the same band gaps as their rodlike counterparts, and nicely, the gap consistency of the ZnS tube and rod also proves the purity of the tube; otherwise, the ZnS tube containing ZnO would show a bandgap similar to that of ZnO/ZnS cable. The ZnO/ZnE (E = S, Se, Te) cables display the efficient gaps associated with that of the narrower-gap component. For example, the E_g of ZnO/ZnS cables is measured to be 3.25 eV, equal to that of ZnO rods; the E_g of ZnO/ZnSe cables is 2.65 eV, same as that of ZnSe rods; and the same E_g value, 2.24 eV, for both ZnO/ZnTe cables and ZnTe rods. These results indicate that both the electron and hole are confined in the same region, core (in case of ZnO/ZnS cables), or the sheath (in cases of ZnO/ZnSe and ZnO/ZnTe cables), which is the character of type-I excitons.[26,27] That is to say the band gap of the ZnO/ZnE heterostructure is tunable via covering a ZnE sheath on the ZnO. These observations are comparable to the report of CdSe/ZnE (E = S, Se) core/shell quantum dots, which only show the absorption band edge of CdSe core.[28,29]

3.5. General Chalcogen Conversion. The successful syntheses and morphology characterizations of three zinc chalcogenides ZnE (E = S, Se, Te) and the heterostructural ZnO/ZnE cables nicely demonstrate the generality and the morphology controllability to some degree of the chalcogen conversion approach in this article. From the light sulfide to the heavy telluride, the corresponding chalcogenidation process is getting difficult because of the increase of both reaction temperature and time. The reaction involving in situ boron chalcogenides is thermodynamically favorite. For one

(18) Okamoto, H. *Phase Diagrams for Binary Alloys; ASM International*, 2000.
(19) Buffat, P.; Borel, J. P. *Phys. Rev. A* **1976**, *13*, 2287–2298.
(20) Lai, S. L.; Guo, J. Y.; Petrova, V.; Ramanath, G.; Allen, L. H. *Phys. Rev. Lett.* **1996**, *77*, 99–102.
(21) Pankove, J. I. *Optical Processes in Semiconductors*; Dover Publications: New York, 1971.
(22) Kortum, G. *Reflectance Spectroscopy: Principles, Methods, Applications*; Springer-Verlag: New York, 1969.
(23) Ueda, K.; Hosono, H. *J. Appl. Phys.* **2002**, *91*, 4768–4770.
(24) Schorr, S.; Riede, V.; Spemann, D.; Doering, T. *J. Alloys. Compd.* **2006**, *414*, 26–30.
(25) Bhargava, R. *Properties of Wide Bandgap II-VI Semiconductors*; INSPEC, The Institution of Electrical Engineers: London, 1997.
(26) Voisin, P.; Bastard, G.; Voos, M. *Phys. Rev. B* **1984**, *29*, 935–941.
(27) Zhang, F. C.; Luo, H.; Dai, N.; Samarth, N.; Dobrowolska, M.; Furdyna, J. K. *Phys. Rev. B* **1993**, *47*, 3806–3810.
(28) Kuno, M.; Lee, J. K.; Dabbousi, B. O.; Mikulec, F. V.; Bawendi, M. G. *J. Chem. Phys.* **1997**, *106*, 9869–9882.
(29) Malik, M. A.; O'Brien, P.; Revaprasadu, N. *Chem. Mater.* **2002**, *14*, 2004–2010.

molar targeted ZnE based on the reaction (I), the change of the Gibbs energies is

$$\Delta G^\circ = \frac{1}{3}\Delta_f G^\circ(B_2O_3) + [\Delta_f G^\circ(ZnE) - \Delta_f G^\circ(ZnO)] \quad (3)$$

Note that the item in the square brackets is equal to the energy change of eq II, in which B is not involved, that is,

$$ZnO + E \rightarrow ZnE + \frac{1}{2}O_2 \quad (II)$$

The values of $\Delta_f G°$(ZnE) are in a decrease series, −190.1, −154.9, and −115.3 kJ/mol, for E = sulfur, selenium, and tellurium, respectively.[30] Because all of these values are significantly smaller than $\Delta_f G°$(ZnO), −320.5 kJ/mol,[30] the reaction (II) is thermodynamically nonspontanous. On the contrary, the reaction (I) is spontaneous because of the rather large $\Delta_f G°(B_2O_3)$ (−1181.5 kJ/mol).[30] Furthermore, an enhanced energy requirement is found from sulfidation to telluridation, which is consistent with the experimental results. Except zinc chalcogenides, we have also successfully made other metal chalcogenides recently, such as rare-earth and transition-metal chalcogenides (La, Nd, Gd, V, Nb, Ta, and Ag) as well as p-block element chalcogenides (Sb and Bi).

The morphologies of the products reported here could be controlled to some degree according to two aspects as followed. One would be the shape resemblance between the final chalcogenides and the initial oxide, that is rods-to-rods conversions; another the design of the core/sheath cables and hollow tubes, that is rods-to-cables-to-tubes developments. Similar to previous report,[9] a self-sacrificing template process might be proposed. That is, the S^{2-}, Se^{2-}, or Te^{2-} diffused into ZnO rods to exchange O^{2-}; the initial ZnO rods served as sacrificial templates to confine the growth of the ZnE, and thus the shape preservable conversions occurred. Also, the sharp XRD peaks of both ZnE and ZnO of the cables suggest the coexistence and the good crystallization of ZnE. Importantly, the capture of the intermediate ZnO/ZnE cables provides substantial evidence for such self-sacrifice process that goes through an exterior-to-interior process and terminates until the ZnO templates are totally consumed. The degree of such ZnO-to-ZnE conversion is sensitive to reaction temperature, time, or loading stoichiometry. Such a method is also able to produce complicated heterostructures, such as double-sheathed cables of ZnO/ZnTe/ZnS (core/sheath/sheath). More work is ongoing.

(30) Barin, I. *Thermochemical Data of Pure Substances*, 3rd Ed.; Wiley-VCH Verlag GmbH: Weinheim, 1995.

4. Conclusion

Three types of zinc chalcogenides ZnE rods and their derivative ZnO/ZnE cables and ZnE tubes (E = S, Se, Te) have been made by the boron-chalcogen conversions. The shape resemblance between ZnE product and ZnO reactant suggests a morphology retentive process. The ZnO-to-ZnE conversion is a ZnO-sacrifice process via an exterior-to-interior erosion route, which is substantiated by the formation of ZnO/ZnE cables. The optical gaps of the as-synthesized ZnE rods agree with those of the corresponding bulk materials, and the ZnO/ZnE cables exhibit type-I excitonic localization character. The boron-chalcogen conversion approach in this article does not involve expensive or toxic organic agents, requires a mild reaction condition, and provides relatively facile morphology controllability. We strongly believe that such method will find wider applications in the fields of nanomaterial synthesis and heterostructure design.

Acknowledgment. This research was supported by the National Natural Science Foundation of China under Projects (20521101, 20773130, 20733003, 20803080), the State Key Laboratory Science Foundation (070023 and 050097), and the "Key Project from FJIRSM" (SZD07004), the "Key Project from CAS" (KJCX2-YW-H01) and the Knowledge Innovation Program of CAS.

IC8005053